Saturn's Small Inner Satellites: Clues to Their Origins

C. C. Porco,[1]* P. C. Thomas,[2] J. W. Weiss,[1] D. C. Richardson[3]

AUTHORS' SUMMARY

Before Voyager 1 arrived at Saturn in 1980, it was thought that the icy particles composing Saturn's rings were the detritus left over from the planet's formation and that strong tidal forces close to the planet prevented them from aggregating to solids much bigger than a few meters across. The Voyager spacecraft discovered small moons orbiting within and just outside the main rings, and made observations that suggested a ring mass equivalent to that of Saturn's 400-km-wide icy moon Mimas. These and other Voyager findings led many scientists to conclude instead that Saturn's rings formed by the catastrophic collisional disintegration of one or several large icy bodies, perhaps preexisting moons. The resulting debris would have quickly settled into the equatorial plane to form a thin disk. It was possible that the different major rings—A, B, and C—formed from different progenitor bodies and therefore were of different ages.

However, Voyager results also implied that a Mimas-sized moon would survive without collisional disruption for so long that any ring-forming event producing that much debris would have had to happen in the early days of the solar system, ~4.5 billion years ago. Hence, ring B, by far the most massive, might be that old. Ring A, with less mass requiring a smaller, more easily disrupted progenitor body, might have formed more recently (1). The presence of moons 30 km in diameter near the outer part of the A ring, such as Pan and Atlas, remained a puzzle: The lifetimes of such small bodies against collision were expected to be shorter still. If disrupted since the A ring's formation, they must have reformed. But how could they do so in the presence of strong planetary tides? It was therefore deemed likely that the small, irregularly shaped moons within and around the rings were shards left over from the original breakup of the rings' progenitor body (or bodies) (2). Even the more distant, small moons of Saturn's major satellites Tethys and Dione were expected to be irregular chips off their larger co-orbital companions.

Divining the origin and evolution of Saturn's entire ring-satellite system was one of the principal goals of the Cassini mission. Cassini has surveyed the rings (within the orbit of Titan) for small bodies missed by Voyager and gathered information on their physical characteristics and orbits. Images have yielded sizes and shapes; masses have been determined through observed gravitational effects on other moons or on the rings.

Here, we show that the ring-region moons have high porosities and low densities, about half the density of water ice. Other Cassini results (3) imply that the ring particles themselves must have a similar low density. Beyond about the orbit of the F-ring shepherd Pandora, where tidal effects weaken, accretion of such porous material can proceed easily. So whether Janus, Epimetheus, or any of the other, much smaller, more distant moons were formed entirely from aggregation of smaller fragments or are monolithic collisional shards, or somewhere in between is unknown. However, closer to the planet, we find that spontaneous, unseeded aggregation of porous particles, even if broadly distributed in size, to form large, homogeneous kilometer-sized bodies is not feasible.

Instead we suggest, and computer simulations support, that the moons Pan and the newly discovered Daphnis (both within the outer A ring), Atlas (just beyond the A ring), and even Prometheus and Pandora (a few thousand kilometers farther out) all likely grew to their present sizes by the accumulation of porous ring material onto massive, denser cores that were one-third to one-half the present-day sizes of the moons. Although the cores themselves may be collisional shards, the present moons in their entirety cannot be. The cores of Pan and Daphnis were likely large enough to open their respective gaps in the rings, and their growth was larg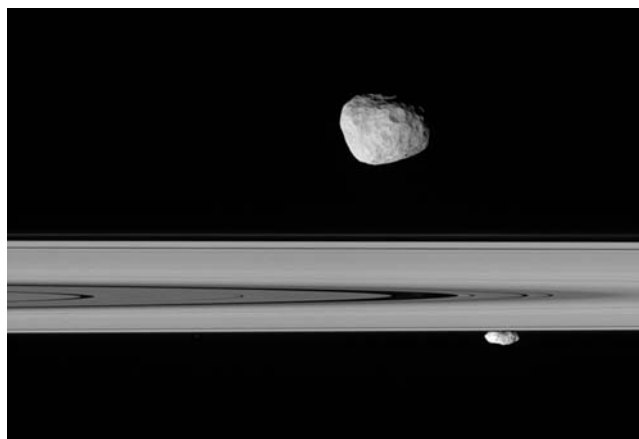ely finished before the gaps were cleared. A secondary stage of accretion apparently formed the equatorial ridges of Pan and Atlas (4), and presumably Daphnis as well, after the disk had thinned to its present ~20-m thickness.

How far in the past all this took place is hard to say, and depends on when and whether Pan and Daphnis were disrupted after their initial formation. However, if they suffered any disruptions at all, their cores must have remained more or less intact, or reformation would have been impossible. Perhaps the thick porous blankets of material surrounding these cores today has protected them from being blown to bits, because porous material can absorb impacts with little damage to the underlying structure (5). It remains to be tested whether the surfaces of Pan and Daphnis and the other moons in the ring region have the same composition as the rings, which would support this story. Also, crater size-frequency distributions on the larger saturnian satellites, especially Iapetus, will clarify how frequently collisions have occurred within the saturnian system, telling us whether the A ring is likely to be young and its small moons have been blasted apart and reaggregated since their original formation, or whether the whole system has been around since the dawn of the solar system.

View from the Cassini spacecraft of Saturn's moon Janus (about 190 km across) on the near side of the rings and Prometheus (about 120 km across) on the far side. Both moons have a low density. Analytical results and computer simulations imply that Prometheus, and perhaps Janus, have grown by accumulating porous ring debris around a relic core.

Summary References
1. L. Esposito, *Icarus* **67**, 345 (1986).
2. B. A. Smith *et al.*, *Science* **215**, 505 (1982).
3. M. Tiscareno *et al.*, *Astrophys. J.* **651**, L65 (2006).
4. S. Charnoz, A. Brahic, P. C. Thomas, C. C. Porco, *Science* **318**, 1622 (2007).
5. E. Asphaug *et al.*, *Nature* **393**, 437 (1998).

FULL-LENGTH ARTICLE

Cassini images of Saturn's small inner satellites (radii of less than ~100 kilometers) have yielded their sizes, shapes, and in some cases, topographies and mean densities. This information and numerical *N*-body simulations of accretionary growth have provided clues to their internal structures and origins. The innermost ring-region satellites have likely grown to the maximum sizes possible by accreting material around a dense core about one-third to one-half the present size of the moon. The other small satellites outside the ring region either may be close to monolithic collisional shards, modified to varying degrees by accretion, or may have grown by accretion without the aid of a core. We derived viscosity values of 87 and 20 square centimeters per second, respectively, for the ring material surrounding ring-embedded Pan and Daphnis. These moons almost certainly opened their respective gaps and then grew to their present size early on, when the local ring environment was thicker than it is today.

The first close views of the small saturnian ring-region satellites Atlas, Prometheus, Pandora, Janus, and Epimetheus came as a result of the Voyager flybys in the early 1980s (*1*, *2*). Voyager images, generally of spatial resolutions coarser than ~2 km/pixel, yielded approximate sizes and albedos. Estimated normal reflectances of ≥ ~0.5 indicated icy rather than rocky compositions (*3*).

The Voyager-era view of the origin of Saturn's rings (*2*, *4*) called for the catastrophic breakup of one or several large icy bodies within the Roche zone of the planet—the boundary within which like-sized bodies cannot accrete owing to the differential gravity from the planet. However, smaller particles within the Roche zone have no difficulty accreting onto bigger bodies [e.g., (*5–7*)]. A progenitor body might have been a recently formed moon that evolved into the Roche zone through aerodynamic drag with the remains of the proto-saturnian nebula before it completely dissipated, or a body that had been captured into orbit around Saturn. The debris from the disruption event(s) became progressively ground down in mutual collisions to create a swarm of particles having a size distribution expected from collisions. The largest collisional shards, which for a system of ice particles would be roughly ~10 km in diameter (*4*), presumably were spared this fate by opening gaps in the rings and terminating their own erosion, assuming that the velocity dispersion of the particles had reduced the ring thickness to a size comparable to the size of the shards.

Other small moons throughout the Saturn system were also generally thought to be collisional shards (*2*). Janus and Epimetheus, occupying as they do essentially the same orbit, were thought to be the two major remnants of a catastrophic disruption of a single progenitor body. Farther from the planet, the small Trojans of Dione and Tethys (Hellene, Calypso, and Telesto)

were believed to be chips off their parent moons, Dione and Tethys, or even off the other large saturnian moons, that were then caught into resonance with Dione and Tethys.

The Imaging Science experiment (*8*) on the Cassini spacecraft has imaged these eight bodies, plus Pan in the Encke gap of the A ring, at image scales better than 1 km/pixel (Figs. 1 and 2). It has discovered three very small moons—Methone, Anthe, and Polydeuces—and has recovered one, Pallene, previously discovered by Voyager, all within the main satellite system; it has also found Daphnis within the Keeler gap of the outer A ring (*9–11*). Cassini has also had a close encounter with one of them, Polydeuces. Image analyses have yielded sizes, shapes, topography, and in some cases masses and, hence, densities.

With this information in hand, we have examined these bodies for similarities and trends in physical characteristics, and compared them to numerical simulations of accretion from a system of particles.

Data and reduction methods. The image analysis technique chosen to measure the size and shape of a given satellite depends on the spatial resolution and coverage of a particular body (*12–15*). The moons' measured and modeled physical characteristics (Table 1) include the semi-axes of an ellipsoid that provides the best fit to the shape. (The observed shape is the collection of measured $\{x,y,z\}$ coordinates of each grid point on a 5° × 5° latitude-longitude grid on the moon's surface.) These semi-axes may give slightly different volumes than those derived directly from the shapes because of imprecision in fitting simple analytic functions to complex natural forms. The moons' mean densities were computed using the actual observed volumes and the best measurements of masses for those moons for which masses have been determined (*16*).

The topography of those moons for which we have reliable shapes, masses, and spin states has also been calculated (Fig. 3). [For completeness, we include topographic models for those moons imaged at sufficient resolution and coverage; we assume an internal density where masses are unavailable (figs. S1 to S3).] Pan and Atlas are distinguished from the rest by distinct, longitudinally asymmetric, equatorial ridges delineated by concavities in the moons' limb profiles (Figs. 2 and 3).

Analysis. We compared the observed satellite properties with those expected for gravitationally bound agglomerations of particles ("rubble piles") that have formed by accretion. Such loose accumulations might be expected to have the shape of the Roche lobe (*5*, *17*). Material can no longer accrete onto a body because of gravity alone once it reaches the size of its Roche lobe. We define the critical density as the density of a body that entirely fills its Roche lobe:

$$\rho_{crit} = \frac{3M_p}{\gamma a_{orbital}^3} \qquad (1)$$

where M_p is the mass of the planet, $a_{orbital}$ is the semimajor axis of the orbit, and γ is a dimensionless shape parameter so that the volume of the moonlet is γa^3, where a is the long semi-axis. For the Roche lobe,

$$\gamma = \frac{2\pi \ln(2+\sqrt{3})}{3\sqrt{3}} \approx 1.59 \qquad (2)$$

For a sphere, $\gamma = 4\pi/3$. Roche lobe dimensions for each moon whose mass is known are given in Table 1. The long semi-axis, a_R, points toward the planet, and the "perpendicular" axis, c_R, lies perpendicular to the orbit plane. The axis ratios for the Roche lobe are $a_R:b_R:c_R = 3:2:2$. For the computation of the critical density, we use the volume of a Roche lobe appropriate for a point-mass source.

Table 1 reveals that the observed long axes of Pan, Daphnis, Atlas, and Prometheus are within 15% of the long axis of the Roche lobe for a body of the given mass at the satellites' orbit. The trend breaks with Janus and Epimetheus, the co-orbital moons, which are much more discrepant in size. The inner satellites have surprisingly low densities: ~0.4 to 0.6 g cm^{-3} (Table 1). The densities of the innermost of these moons are all approximately equal to the critical density at that distance, whereas farther from Saturn, the densities of Janus and Epimetheus are not. These comparisons immediately suggest a formation scenario (for at least the innermost moons) of growth by accretion of material until the critical density is reached, at which point the moon more or less fills its Roche lobe.

Numerical simulations. We have examined accretion into a "rubble pile" with the use of a numerical code that realistically simulates the behavior of ring particles in a patch of fixed dimensions in orbit around Saturn, inclusive of collisional and self-gravitational effects (*18*, *19*). In this patch, we embedded, in turn, solid cores with radii of 12.5 and 25 m and internal densities of 0.9 g cm^{-3} appropriate for solid water ice. We chose particle disk characteristics—optical depth and surface mass density—believed to be representative of Saturn's A ring (*20*, *21*). The ring particles were given a differential power-law size distribution, $dN(r) \propto r^{-q}dr$, with $q \sim 3$ and radii r ranging from 0.3 to 5 m (*22*), a mass density of 0.4 g cm^{-3} reasonable for porous icy bodies, and elastic properties expected for ice (*23*). The size of the patch was chosen to be at least 10 times the final size of the moonlet's Roche lobe to minimize interactions between the moonlets and their mirror images in

[1]Cassini Imaging Central Laboratory for Operations (CICLOPS), Space Science Institute, 4750 Walnut Street, Boulder, CO 80301, USA. [2]Center for Radiophysics and Space Research, Cornell University, Ithaca, NY 14853, USA. [3]Department of Astronomy, University of Maryland, College Park, MD 20742, USA.

*To whom correspondence should be addressed. E-mail: carolyn@ciclops.org
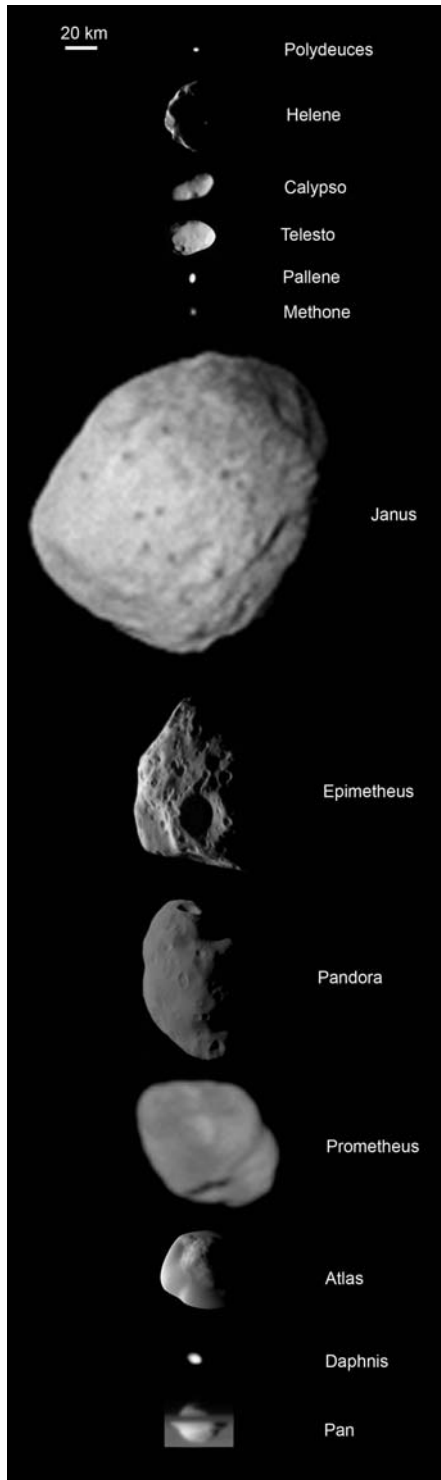
Fig. 1. The highest-resolution images of all the small saturnian moons, except Anthe (between Methone and Pallene), shown to the same scale and in order of distance from Saturn. Pan is transiting Saturn and is partially occulted by the edge-on rings.
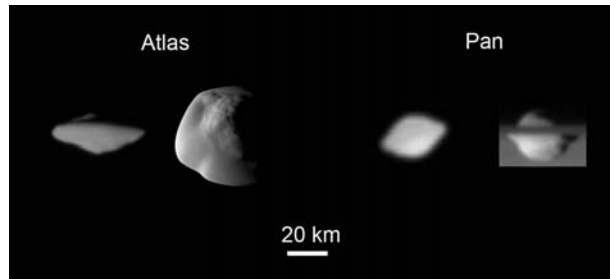
Fig. 2. The highest-resolution images of Pan and Atlas, showing their distinctive "flying saucer" shapes, owing to equatorial ridges not seen on the other moons. From left to right: a view of Atlas' trailing hemisphere, with north up, at a spatial scale of ~1 km/pixel; Atlas seen at ~250 m/pixel from mid-southern latitudes, with sub-Saturn hemisphere pointing up and leading hemisphere to the left; Pan's trailing hemisphere seen at ~3 km/pixel from low southern latitudes; an equatorial view, with Saturn in the background, of Pan's anti-Saturn hemisphere at ~1 km/pixel. On Atlas, the ridge extends 20° to 30° in latitude on either side of the equator; on Pan, its latitudinal extent is 15° to 20°. Atlas shows more asymmetry than Pan in having a more rounded ridge in the leading and sub-Saturn quadrants. The heights of the ridges can be crudely estimated by assuming ellipsoidal shapes that lack ridges and vary smoothly across the equator (fig. S4). Heights of Atlas' ridge range from ~3 km (270°W) to 5 km (180° and 0°W); Pan's ridge reaches ~4 km at 0°W and is ~1.5 km over most of the rest of the equator. The ridge represents ~27% of Atlas' volume and 10% of Pan's volume.

ing new particles—and its effective bulk density dropped to the critical density (i.e., the value where it exactly fills its Roche lobe). The a, b, and c axes of the simulated moonlet were in a ratio of approximately 6:4:3, close to the effective Roche lobe axes ratio of 6:4:4 (Fig. 4). The discrepancy may be due to finite particle size effects in our simulations, where some of the accreted particles are smaller than the core by factors of only 2 to 5. An alternative explanation is that the particles with low relative velocity tend to enter through the inner and outer Lagrange points at the moonlet's equator and then migrate to different longitudes as well as higher latitudes, and this process may not be 100% effective at filling the Roche lobe in the perpendicular direction. The low bulk density and implied global porosities of the moonlet (~30 to 65%) are consistent with porosities inferred for many asteroids, commonly 20 to 60% (24), and for icy Hyperion, ~43% (25).

Discussion. The expected final size of a growing moon with a long semi-axis a, relative to the initial core with radius R_c, can be calculated as

$$\frac{a}{R_c} = \left(\frac{4\pi}{3\gamma}\frac{\rho_c - \rho_m}{\rho_{crit} - \rho_m}\right)^{1/3} \quad (3)$$

where ρ_{crit} is the critical density, ρ_c is the density of the core, and ρ_m is the density of the mantle of material accreted around the core. (Note that ρ_m is equal to the bulk density of the particles, ρ_p, times their filling factor in the mantle; this equation is applicable only when $\rho_m < \rho_{crit}$.) We define mantle "macroporosity" to be $1 - (\rho_m/\rho_p)$, a measure of the degree of packing of the accreted material. The macroporosity of the accreted material, with a bulk density of $\rho_p = 0.4$ g cm^{-3} in our simulations, is ~65%.

Particles with bulk densities very near or below the critical density of 0.4 g cm^{-3} will not accrete material, and homogeneous rubble piles with no central mass concentration are not even stable against tidal shear in the ring region—hence the need for a core of larger density to begin the process of accretionary growth to a stable moon. If the core is a kilometer-sized collisional shard resulting from the breakup of a

bigger icy progenitor ring body (4), it is reasonable to assume that its density might be somewhere between 0.5 and 0.9 g cm^{-3}. We find that for this plausible range of core densities, the ring-region moons had to begin with cores that were approximately one-half to one-third the size of the final body (Fig. 5). In that case, neither ~40-km-radius Prometheus nor ~4-km-radius Daphnis could have begun with a 10-m-radius core.

Despite the gross difference in the core sizes compared (i.e., 12.5 m versus tens of kilometers), the ratio of the escape speed from the moonlet to the tidal shear across it, $V_{esc}/\Omega R$, is a constant for the same mean density, independent of moonlet size. ($V_{esc}/\Omega R$ is a measure of the strength of the moon's gravity pulling on a particle relative to the tidal forces that tend to keep particles from accreting.) This is also suggested by the identical results we achieved when we doubled the core size in our simulations (Fig. 5). Thus, for the purposes of investigating the general character of accretion, our numerical results are essentially scale-invariant and should apply to much larger bodies at the same orbital distance from Saturn, although nonspherical ring particle shapes and finite size effects may alter the mantle porosity somewhat from small to large sizes.

The observed moons deviate from exact Roche lobe shapes. Indeed, almost all of them have intermediate axes larger than those of their Roche lobes (Table 1). For Pan and Atlas, their shapes are more like flying saucers (Fig. 2), and even the ridgeless forms of Pan and Atlas show a departure from the classic Roche shape (fig. S4). The point-source assumption in computing the Roche lobe shape, which might be expected to contribute to these discrepancies, in fact contributes very little (26). Other processes, however, can affect the detailed shapes of an accreting satellite. Those that work to make the surface approximately an equipotential, such as fluid behavior or downslope transport of loose material, generally fail for objects less than 100 km in radius (27). Departures from a pure Roche lobe shape might instead be expected as a result of the details of accretion. For example, particles carrying sufficient kinetic energy can strike

neighboring virtual cells (which are needed to provide the boundary conditions at the patch edges).

As expected, the core accreted particles until a statistical equilibrium was reached—as many particles were accreted as were dislodged by incom-

Table 1. Characteristics of Saturn's small moons. Orbital distances from Saturn, $a_{orbital}$, are from (29) for all moons except Anthe (11), Telesto, Calypso, and Helene; orbital distances of the latter three are taken from the JPL ephemeris file SAT252. Masses are determined from orbital integrations [i.e., satellite-satellite perturbations (27)] or, for Pan (9) and Daphnis (32), from the effects of the moons on the rings. Mean radius, r_m, is that for a sphere having the same volume as the observed moon, except for Anthe, whose mean radius has been estimated from its brightness (11). Axes a, b, and c are those of the best-fit model ellipsoid; a_R, b_R, and c_R are the Roche lobe axes, computed using the moons' masses and assuming a point-mass source. Critical densities, ρ_{crit}, are computed as described in the text. Moons' estimated densities, ρ, are obtained from satellite masses and observed shapes. Fitted ellipsoid dimensions for Pan and Atlas with ridges removed are 15.9, 15.1, and 10.7 km, and 16.9, 16.0, and 9.3 km, respectively.

Satellite	$a_{orbital}$ (km)	Mass (× 10^{19} g)	r_m (km)	a (km)	b (km)	c (km)	± δa, δb, δc (km)	c/a	a_R (km)	$b_R = c_R$ (km)	a/a_R	ρ_{crit} (g cm^{-3})	ρ (g cm^{-3})	ρ/ρ_{crit}
Pan	133,584	0.495 ± 0.075	14.2 ± 1.3	17.4	15.8	10.4	2.0, 1.3, 0.84	0.60	19.1	12.7	0.91	0.45	0.41 ± 0.15	0.92 ± 0.32
Daphnis	136,504	0.0084 ± 0.0012	3.9 ± 0.8	4.5	4.3	3.1	0.8, 0.8, 0.9	0.69	4.9	3.2	0.93	0.42	0.34 ± 0.21	0.80 ± 0.50
Atlas	137,670	0.66 ± 0.06	15.1 ± 1.4	20.9	18.1	8.9	1.4, 2.5, 0.8	0.43	21.6	14.4	0.97	0.41	0.46 ± 0.10	1.12 ± 0.24
Prometheus	139,380	15.67 ± 0.20	43.1 ± 2.7	66.3	39.5	30.7	3.2, 3.2, 2.0	0.46	62.9	41.9	1.05	0.40	0.47 ± 0.065	1.18 ± 0.17
Pandora	141,720	13.56 ± 0.23	40.3 ± 2.2	51.6	39.8	32.0	1.8, 2.1, 2.9	0.62	61.0	40.7	0.85	0.38	0.50 ± 0.085	1.32 ± 0.23
Epimetheus	151,410	53.07 ± 0.14	56.7 ± 1.9	58.0	58.7	53.2	2.5, 3.2, 0.8	0.92	102.7	68.4	0.57	0.31	0.69 ± 0.13	2.25 ± 0.42
Janus	151,460	188.91 ± 0.50	89.6 ± 2.0	97.4	96.9	76.2	2.9, 2.2, 1.2	0.78	157.4	105	0.62	0.31	0.63 ± 0.063	2.03 ± 0.21
Methone	194,440	–	1.6 ± 0.6	–	–	–	0.6	–	–	–	–	0.15	–	–
Anthe	197,700	–	~1	–	–	–	–	–	–	–	–	0.14	–	–
Pallene	212,280	–	2.2 ± 0.3	2.6	2.2	1.8	0.4, 0.3, 0.2	0.69	–	–	–	0.11	–	–
Telesto	294,710	–	12.4 ± 0.4	15.7	11.7	10.4	0.6, 0.3, 0.3	0.66	–	–	–	0.04	–	–
Calypso	294,710	–	10.6 ± 0.7	15.0	11.5	7	0.3, 2.3, 0.6	0.47	–	–	–	0.04	–	–
Polydeuces	377,200	–	1.3 ± 0.4	1.5	1.2	1.0	0.6, 0.4, 0.2	0.67	–	–	–	0.02	–	–
Helene	377,420	–	16.5 ± 0.6	19.4	18.5	12.3	0.2, 1.0, 1.0	0.63	–	–	–	0.02	–	–

a surface and stick because of cohesive and frictional forces, even if the impact site has a considerably higher gravitational potential than other locales on the surface. Alternatively, hyper-velocity impacts may form large craters, redistribute material around the surface (or eject it entirely), and in general compete with low-speed accretion and consequently lead to deviation from an equipotential surface. Accretion of particles with low relative velocity that are essentially coplanar with the satellite and are therefore on low-inclination orbits, might also build up the moon's intermediate axes long before the Roche lobe has been "filled." Finally, a moon's detailed orbital motion can determine where around the midsection the material will ultimately land. The equatorial ridges of Pan and Atlas and their specific longitudinal asymmetries can be explained by a post-formation, late-stage accretion (28) from a vertically thin disk. The details depend on the eccentricities and inclinations of these two moons (29). (Daphnis too may sport a ridge, owing to accretion from the thin rings, that Cassini may reveal in future observations.) Thus, it is not surprising that the moons do not have exact Roche lobe shapes.

We tested the degree to which interior models with dense cores move the surfaces toward equipotentials by calculating (12) the surface potentials and the effective gravitational topography on the four ring moons, using their observed shapes and assuming a central core of 0.9 g cm^{-3} and a mantle of density 0.15 g cm^{-3} (Fig. 3). The gravitational topography on the ring-region moons Pan, Atlas, Prometheus, and Pandora reaches a few kilometers, or modest fractions of the mean radii. The very low values of gravity on the Saturn and anti-Saturn equatorial regions indicate that these objects are in fact near the limit of accretion in those locales, as expected. These features are not unique to "core" interior models: Assuming a uniform-density interior produces comparable gravitational topography (Fig. 6). However, because a dense core is required to start the accretion process, the observations, core models, and simulations are consistent with a formation scenario, for at least the innermost moons, of growth by accretion around a dense core to the maximum possible size (and minimum critical density), wherein the overall Roche lobe conditions and the varied dynamics of impacting particles dominate any possible effects due to surface processes such as downslope motion.

If this accretionary growth model is correct, we can now add an additional factor to the dynamic history of ring-embedded moons such as Pan and Daphnis, which currently maintain gaps—Encke and Keeler, respectively—in Saturn's outer rings. The mass of a ring-embedded moonlet required to open and maintain a narrow gap at a given orbital radius can be found by balancing the viscous ring torque with the torque exerted by a satellite on the gap edge (30):

$$\mu^2 = \frac{3\pi\nu}{0.84(a_{orbital})^2\Omega}\left(\frac{w}{a_{orbital}}\right)^3 \quad (4)$$

where Ω is the orbital frequency at semimajor axis $a_{orbital}$, μ is the ratio of the mass of the moonlet to the mass of Saturn, w is the half-width of the gap, and ν is the viscosity of the ring. For Pan and Daphnis to maintain their present gaps, the ring viscosities must be $\nu \sim 87$ cm^2 s^{-1} for Pan and $\nu \sim 20$ cm^2 s^{-1} for Daphnis. Using these viscosities, we can find the minimum mass required to open the Encke and Keeler gaps. That point is reached when the moon grows to a mass where the gap width, maintained by its overlapping Lindblad resonances at the gap's edge, exceeds the moon's Roche lobe (assuming that the ring's thickness is not much larger than the moon).

Replacing w with the Roche lobe radius $[a_{orbital}(\mu/3)^{1/3}]$, we obtain

$$\mu = \frac{\pi\nu}{0.84(a_{orbital})^2\Omega} \quad (5)$$

Using the viscosities derived above produces a minimum Pan mass for opening the Encke gap of $GM_P \sim 5.5 \times 10^{-7}$ km^3 s^{-2}, yielding a Roche lobe semi-axis $a \sim 2$ km; for Daphnis and the Keeler gap, $GM_D \sim 1.2 \times 10^{-7}$ km^3 s^{-2} and $a \sim 1$ km. Daphnis' mass today is 40 times this minimum for the Keeler gap; Pan's mass is 600 times the minimum to open the Encke gap. Their original cores must have been between 1.8 and 3 km in radius for Daphnis, and ~8 to 12 km for Pan, depending on the core density (Fig. 5). It is likely that both bodies, but especially Pan, opened their gaps before growing to their final sizes (and dropping to their critical density).

In order for Pan and Daphnis to grow from small cores to the sizes they are today, both the initial gap-opening and accretionary epochs for these moons must have occurred during a time when the local debris disk they were embedded in was at least comparable to the final size of the moon and not as vertically thin (~20 m) as Saturn's present rings—that is, very early in the history of the outer A ring. (By analogy, the same would be true even for Atlas, Prometheus, and Pandora.) Because times for collapse to a thin disk are short (4), the accretion stage must also have occurred rapidly. A later secondary accretionary stage for Pan and Atlas, after the local disk had thinned to its present state but was still amply populated, was likely responsible for adorning these two moons with the distinct equatorial ridges we see today (28).

The possibility that all these ring-region moons were catastrophically disrupted and reaccreted, perhaps several times, during the lifetime of the A ring (2) does not fundamentally alter the above

sequence of events, but only resets the time of last occurrence. This assumes that the dense cores more or less survived the disruption and were therefore available to initiate the next accretionary epoch. The thick shells of ring material surrounding the cores may in fact have protected them from breakup (*31*). In this case, the debris clouds from which today's observed moons coalesced would simply consist of material recycled from their most recent disruption.

The discrepancy between the Roche lobe size and the sizes of the more distant moons, such as Janus and Epimetheus, may imply that these moons ran out of ring material before reaching their critical densities and maximum sizes. These moons very likely originated closer to Saturn and, through the torques they exert on the rings, quickly moved out to their present position (*30*). Taking their possible radial migration into consideration, their sizes are still significantly smaller, and their mass densities significantly higher, than one would expect for a Roche lobe–filling body in their general vicinity. If their formation location was more distant than ~148,000 km from Saturn, it is possible that they are entirely accretional in origin, as no core is required for accretion beyond this distance assuming the ring particle mass densities we have adopted here (Fig. 5). However, if they formed within an orbital distance of ~148,000 km from Saturn, they may in fact be the original shards, perhaps modified to some degree by accretion, that resulted from the disruption of their progenitor body (*2*).

Within the observational uncertainties, the tiny satellite-region moons beyond Janus (i.e., Methone, Anthe, Pallene, and Polydeuces) could be any shape. Of the larger Trojans, only Telesto's shape looks Roche-like, and high-resolution images show it to be visibly coated with debris, implying perhaps some accretion. The critical densities at the orbital distances of all these moons are so small that it is exceedingly doubtful that these moons are filling their Roche lobes; such densities imply implausibly high macroporosities approaching ~95%. All these moons, like Janus and Epimetheus, may be original collisional shards that have been modified by accretion to varying degrees by some combination of the processes mentioned above, or they may have formed entirely by accretion without the aid of a dense core.

References and Notes

1. B. A. Smith *et al.*, *Science* **212**, 163 (1981).
2. B. A. Smith *et al.*, *Science* **215**, 505 (1982).
3. P. C. Thomas, J. Veverka, D. Morrison, M. Davies, T. V. Johnson, *J. Geophys. Res.* **88**, 8743 (1983).
4. A. Harris, in *Planetary Rings*, R. Greenberg, A. Brahic, Eds. (Univ. of Arizona Press, Tucson, AZ, 1984), pp. 641–659.
5. D. R. Davis, S. J. Weidenschilling, C. R. Chapman, R. Greenberg, *Science* **224**, 744 (1984).
6. A. R. Dobrovolskis, J. A. Burns, *Icarus* **42**, 422 (1980).
7. R. M. Canup, L. W. Esposito, *Icarus* **113**, 331 (1995).
8. C. C. Porco *et al.*, *Space Sci. Rev.* **115**, 363 (2004).
9. C. C. Porco *et al.*, *Science* **307**, 1226 (2005).
10. C. C. Porco *et al.*, *IAU Circ. 8432* (2004).
11. C. C. Porco *et al.*, *IAU Circ. 8857* (2007).
12. P. C. Thomas, *Icarus* **105**, 326 (1993).
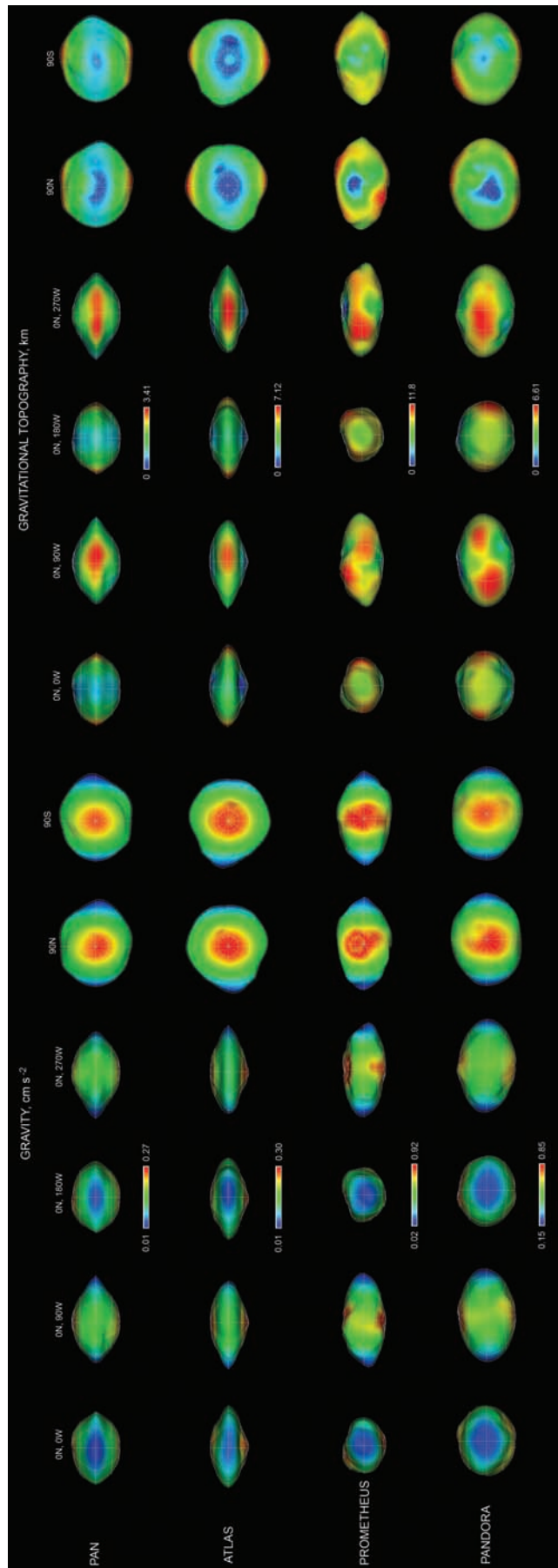13. D. P. Simonelli, P. Thomas, B. T. Carcich, J. Veverka, *Icarus* **103**, 49 (1993).

Fig. 3. Modeled gravitational topography for the ring-region moons Pan, Atlas, Prometheus, and Pandora, assuming core and mantle densities of 0.9 g cm^{-3} and 0.15 g cm^{-3}, respectively. The figures are based on the appropriate spin, tidal forces, and potential energy at the surface. Left panels show magnitude of surface accelerations. Right panels show gravitational topography, which is the potential energy (relative to the south pole) divided by an average acceleration. Views, from left to right, are of the Saturn-facing, leading, anti-Saturn, trailing, northern, and southern hemispheres.
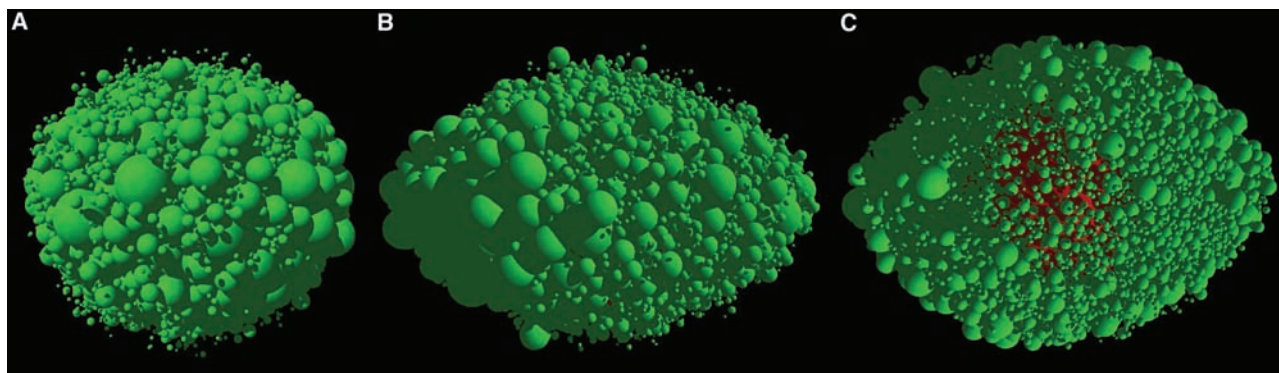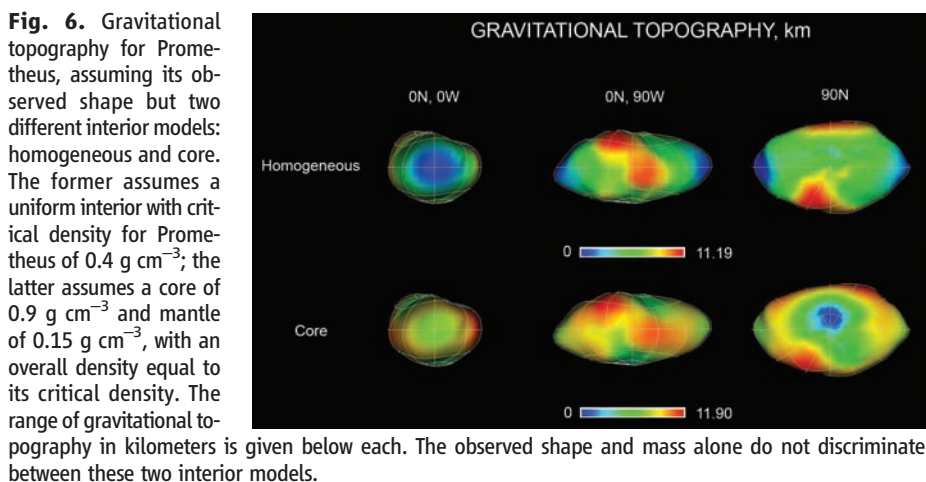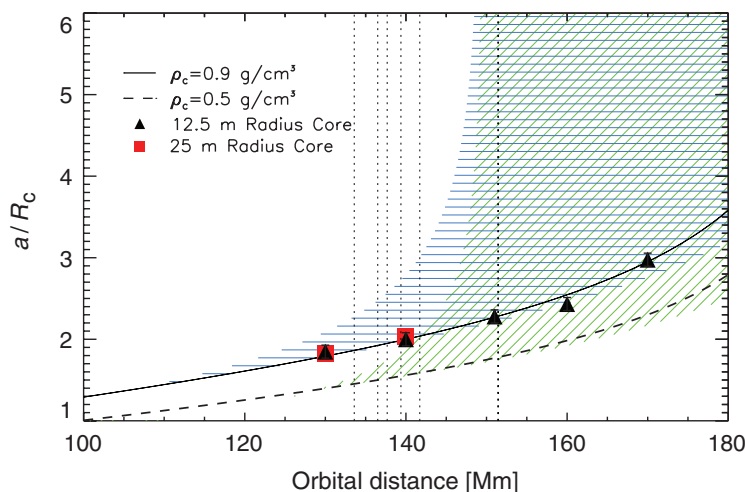
Fig. 4. Ring-patch code simulations with an embedded moonlet of radius 25 m. (**A**) View of the Saturn-facing hemisphere. (**B**) View of the leading hemisphere. (**C**) View from the northern hemisphere, with the leading hemisphere pointing downward. The red region visible in these images is the core, slightly visible in (C). The observed axes ratio in these simulations was 6:4:3, slightly smaller than the classic Roche lobe shape of 6:4:4 in the vertical direction.

Fig. 5. Variation with orbital radius from Saturn of the final relative size of a moon (with respect to the size of the core) growing in a disk of particles with internal bulk mass density of 0.4 g cm^{-3}. Green hatched region is the range of final sizes for a moon with a core of 0.5 g cm^{-3}; blue hatched region, for a moon with a core of 0.9 g cm^{-3}. Both are bounded by mantle porosities of 20% (top) and 70% (bottom), or mantle densities of 0.32 g cm^{-3} and 0.12 g cm^{-3}, respectively. Data points are the simulation results for a core with a radius of 12.5 m (triangles) and 25 m (red squares), a density of 0.9 g cm^{-3}, and a porosity of 65% (or a mantle density of 0.15 g cm^{-3}). Error bars on the simulations are comparable to the size of the symbols and show the statistical variations in the final moonlet size over the last five orbits of the 15-orbit simulations. The solid and dashed black curves are the theoretical predictions for moons with two different core densities and the mantle porosity (~65%) found in all the simulations. The agreement between data and theory confirms the relation used to calculate the hatched regions. Vertical dotted lines signify the locations of the moons considered in this paper: from left to right, Pan, Daphnis, Atlas, Prometheus, Pandora, and Janus/Epimetheus. Beyond ~148,000 km, moonlet growth does not require a dense core; accretion and growth from a debris disk can proceed unaided.

Fig. 6. Gravitational topography for Prometheus, assuming its observed shape but two different interior models: homogeneous and core. The former assumes a uniform interior with critical density for Prometheus of 0.4 g cm^{-3}; the latter assumes a core of 0.9 g cm^{-3} and mantle of 0.15 g cm^{-3}, with an overall density equal to its critical density. The range of gravitational topography in kilometers is given below each. The observed shape and mass alone do not discriminate between these two interior models.

14. P. C. Thomas *et al.*, *Icarus* **135**, 175 (1998).
15. See supporting material on *Science* Online.
16. Masses are unavailable for the Trojans of Tethys (Calypso and Telesto) and Dione (Helene and Polydeuces), as well as the tiny satellite-region moons Methone, Anthe, Pallene, and Polydeuces, because none of these is massive enough to measurably perturb any nearby or resonant moons.
17. J. M. A. Danby, *Fundamentals of Celestial Mechanics* (Willmann-Bell, Richmond, VA, 1992).
18. D. C. Richardson, *Mon. Not. R. Astron. Soc.* **269**, 493 (1994).
19. D. C. Richardson, T. Quinn, J. Stadel, G. Lake, *Icarus* **143**, 45 (2000).
20. J. Colwell, L. W. Esposito, M. Sremcevic, *Geophys. Res. Lett.* **33**, L07201 (2006).
21. M. S. Tiscareno *et al.*, *Nature* **440**, 648 (2006).
22. R. G. French, P. D. Nicholson, *Icarus* **145**, 502 (2000).
23. K. D. Supulver, F. G. Bridges, D. N. C. Lin, *Icarus* **113**, 188 (1995).
24. D. T. Britt, D. Yeomans, K. Housen, G. Consolmagno, in *Asteroids III*, W. F. Bottke, A. Cellino, P. Paolicchi, R. P. Binzel, Eds. (Univ. of Arizona Press, Tucson, AZ, 2002), pp. 485–500.
25. P. C. Thomas *et al.*, *Nature* **448**, 50 (2007).
26. It is reasonable to question the assumption that the moonlets are point masses in calculating the Roche lobe dimensions (shape and critical density) because they are clearly extended bodies. However, no self-gravitating extended body with a homogeneous interior and the low densities found for the moons in this study is even stable in the ring region, and bodies with dense cores and under-dense mantles differ in their dimensions from those of a point-mass Roche lobe by at most ~5%.
27. I. Sharma, J. T. Jenkins, J. A. Burns, *Icarus* **183**, 312 (2006).
28. S. Charnoz, A. Brahic, P. C. Thomas, C. C. Porco, *Science* **318**, 1622 (2007).
29. J. Spitale *et al.*, *Astron. J.* **132**, 692 (2006).
30. P. Goldreich, S. Tremaine, *Annu. Rev. Astron. Astrophys.* **20**, 249 (1982).
31. E. Asphaug *et al.*, *Nature* **393**, 437 (1998).
32. J. W. Weiss, C. C. Porco, M. S. Tiscareno, J. A. Burns, L. Dones, *Bull. Am. Astron. Soc.* **37**, 767 (2005).
33. We thank the staff members of CICLOPS and B. Carcich (Cornell University) for technical support, and L. Dones for fruitful discussions. Supported by NASA Planetary Geology and Geophysics grant NAG5-4451 and the Cassini Project.

Editor's Summary

Article Tools	Visit the online version of this article to access the personalization and article tools: http://science.sciencemag.org/content/318/5856/1602
Permissions	Obtain information about reproducing this article: http://www.sciencemag.org/about/permissions.dtl